Formation Mechanisms and Properties of Semifluorinated Molecular Gradients on Silica Surfaces

Jan Genzer,*,† Kirill Efimenko,† and Daniel A. Fischer‡

Department of Chemical & Biomolecular Engineering, North Carolina State University, Raleigh, North Carolina 27695-7905, and Material Science & Engineering Laboratory, National Institute of Standards and Technology, Gaithersburg, Maryland 20899

Received April 13, 2006. In Final Form: July 22, 2006

The goal of this study is to elucidate the formation of molecular gradients made of semifluorinated organosilanes (SFOs) on flat substrates by using a methodology developed by Chaudhury and Whitesides (*Science* **1992**, *256*, 1539). We use surface-sensitive combinatorial near-edge X-ray absorption fine structure (combi-NEXAFS) spectroscopy to measure the position-dependent concentration and orientation of SFO molecules in SFO molecular gradients on flat silica surfaces. Using the combi-NEXAFS data, we establish the correlation between the fraction of the $F(CF_2)_8$-$(CH_2)_2-$ species on the substrate and the average tilt angle of the $-(CF_2)_8F$ group in the SFO as a function of the deposition gas medium (air vs nitrogen) and the end group around the silicon atom (monofunctional vs trifunctional). In addition, we utilize the gradient geometry to comprehend the mechanism of formation of SFO self-assembled monolayers (SAMs). Specifically, we provide evidence that depending on the nature of the end group in the SFO and the vapor phase the SFO molecules add themselves into the existing SAMs either as individual molecules or as multimolecular complexes.

Introduction

A typical method of adjusting the physicochemical properties of material surfaces involves decorating the surfaces with self-assembled monolayers (SAMs).[1−4] The particular bonding chemistry involved in depositing SAMs depends on the substrate type. For instance, surfaces of certain noble metals (e.g., gold, silver, palladium, platinum, mercury, copper) or semiconductors (e.g., GaAs) can be covered with SAMs whose end group is based on either mercapto or disulfide chemistries.[1−4,5] Alkenes become the choice for modifying hydrogen-terminated (e.g., SiH) surfaces,[6] and alkylphosphonates are known to attach to noble metal-, oxide-, and indium−titanium oxide-based surfaces.[7] Finally, just about any oxide surface can be decorated with organized arrays of SAMs based on organosilane chemistries.

In most instances one is interested in covering the substrates with SAMs in which the spatial distribution of the SAM-forming molecules is homogeneous everywhere on the surface (cf. Figure 1, left panel). For other applications, one may need to prepare SAMs, in which the concentration of the molecules varies spatially across the substrate. To create chemical patterns comprising regions with distinct wettabilities separated via sharp boundaries, one can apply the SAMs on the substrate by utilizing one of many existing soft lithography methodologies.[8] In addition, there may be cases, where one would need to create surfaces with spatially and continuously varying chemistries on substrates (cf. Figure 1, right panel).[9] In such "gradient surfaces", the gradually varying concentration of SAM molecules on the surface produces gradients in wettability, thickness, dielectric constant, and other physicochemical properties. Substrates thus formed will, in turn, find use in several attractive applications, including selective adsorption,[10,11] gradient templating,[12−16] controlled motion of liquid droplets,[17−19] formation of patterns as templates for further processing (i.e., surface-initiated polymerization),[20,21] particle sorting,[22] and many others. In addition to the broad range of

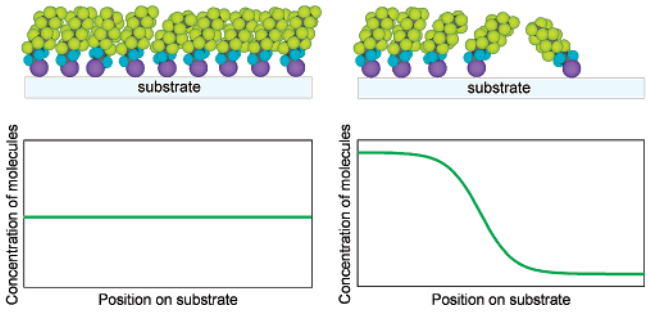

Figure 1. Schematic illustrating molecular organization in homogeneous (left panel) and gradient (right panel) SAMs. While the concentration in homogeneous SAMs is spatially uniform, the concentration in gradient SAMs varies as a function of the position on the substrate.

* To whom correspondence should be addressed. E-mail: Jan_Genzer@ncsu.edu.

† North Carolina State University.

‡ National Institute of Standards and Technology.

(1) Ulman, A. *An Introduction to Ultrathin Organic Films from Langmuir−Blodgett to Self Assembly*; Academic Press: New York, 1991.

(2) Ulman, A., Ed. *Organic Thin Films and Surfaces: Direction for the Nineties, Thin Films*; Academic Press: Boston, 1995; Vol. 20.

(3) Ulman, A. *Chem. Rev.* **1996**, *96*, 1533.

(4) Schreiber, F. *Prog. Surf. Sci.* **2000**, *65*, 151.

(5) Krapchetov, D. A.; Ma, H.; Jen, A. Y. K.; Fischer, D. A.; Loo, Y.-L. *Langmuir* **2005**, *21*, 5887.

(6) Linford, M. R.; Fenter, P.; Eisenberger, P. M.; Chidsey, C. E. D. *J. Am. Chem. Soc.* **1995**, *117*, 3145.

(7) Brewer, S. H.; Brown, D. A.; Franzen, S. *Langmuir* **2002**, *18* 6857.

(8) Zhao, X.-M.; et al. *J. Mater. Chem.* **1997**, *7*, 1069. Qin, D.; et al. *Top. Curr. Chem.* **1998**, *194*, 1. Whitesides, G. M.; Xia, Y. *Annu. Rev. Mater. Sci.* **1998**, *28*, 53. Xia, Y.; et al. *Chem. Rev.* **1999**, *99*, 1823; *Angew. Chem., Int. Ed.* **1998**, *37*, 550.

(9) Bain, C. *ChemPhysChem* **2001**, *2*, 580.

(10) Ruardy, T. G.; Schakenraad, J. M.; van der Mei, H. C.; Busscher, H. J. *Surf. Sci. Rep.* **1997**, *29*, 3.

(11) Clare, B. H.; Efimenko, K.; Fischer, D. A.; Genzer, J.; Abbott, N. L. *Chem. Mater.* **2006**, *18*, 2357.

(12) Bhat, R. R.; Fischer, D. A.; Genzer, J. *Langmuir* **2002**, *18*, 5640.

(13) Plummer, S. T.; Bohn, P. W. *Langmuir* **2002**, *18*, 4142.

(14) Bhat, R. R.; Chaney, B. N.; Rowley, J.; Liebmann-Vinson, A.; Genzer, J. *Adv. Mater.* **2005**, *17*, 2802.

(15) Bhat, R. R.; Genzer, J. *Appl. Surf. Sci.* **2005**, *252*, 2549.

(16) Bhat, R. R.; Tomlinson, M. R.; Genzer, J. *Macromol. Rapid Commun.* **2004**, *25*, 270.

(17) Chaudhury, M. K.; Whitesides, G. M. *Science* **1992**, *256*, 1539.

10.1021/la061016r CCC: $33.50
Published on Web 08/25/2006

applications, there is one extra benefit the gradient geometry can offer. Specifically, the gradient geometry constrains the self-assembly growth into a given direction, which is in contrast to the classical case of "uniform" self-assembly on a substrate, where the incorporation of the molecules in the final SAM takes place at random in all directions.[1−4] Hence, by monitoring how the gradient-forming molecules arrange themselves across the gradient interfacial region, one can gain insight into the mechanisms and nature of self-assembly in organosilane SAMs on surfaces.

Over the past four decades, multiple methodologies leading to the production of gradient surfaces have been conceived and developed.[10,23−25] They are based on either gradually depositing the SAM molecules or by gradually modifying the chemical nature of existing chemically homogeneous surfaces. Since most of the "classical" methods leading to the formation of gradient surfaces were reviewed,[10,23−26] many new techniques have emerged.[27−36] Each technique has its strengths and weaknesses. Moreover, when choosing an optimal gradient-preparation method, one has to consider both the type of starting material (substrate, geometry, chemistry involved) and the final properties of the gradient to be formed (gradient spatial dimension, resistance against surface reconstruction or modification).

One of the most widely used methods in preparing gradient surfaces is based on vapor deposition of low-molecular-weight organosilanes.[17] Since its introduction by Chaudhury and Whitesides more than a decade ago, this method has been used in a variety of case studies involving controlled motion of liquid droplets,[17−19] formation of 2-dimensional nanoparticle gradients,[12] preparation of surface-bound polymer brushes with grafting density gradients,[16,37,38] and others. The technique is based on evaporating organosilane molecules from a diffusing source into a vapor medium. After escaping from the liquid phase, the molecules form a concentration gradient in the vapor phase, eventually land on a substrate, which is placed horizontally next to the diffusing source, and chemisorb by reacting with the surface-bound hydroxyl groups. The concentration of the organosilanes along the substrate decreases as a function of the distance from the diffusing source. The characteristics of the thus formed density gradients of chemisorbed molecules depend on a battery of parameters, including (1) the diffusing geometry (confined vs unconfined), (2) the properties of the diffusing molecules (chemical structure, vapor pressure, flux, nature of the bonding group), (3) the diffusing medium (gas type, humidity, temperature), and (4) the properties of the substrate (continuous vs discontinuous, density of surface-bound hydroxyl groups, temperature).

In our previous paper[39] we have evaluated the effect of the diffusing geometry on the mechanism governing the formation of the wettability gradients. We have provided evidence that, depending on the degree of confinement of the vapor phase, the gradient either forms following a classical diffusion from an infinite source (unconfined system, accomplished by covering the diffusing source with a large, say 2 L, beaker) or develops via propagating front growth (confined system, typically carried out in a small Petri dish). In a subsequent paper we will discuss how gradient formation proceeds in cases involving more than one diffusing source.[40] In this paper we use semifluorinated organosilanes (SFOs) based on $F(CF_2)_8(CH_2)_2-$ (F8H2) functional groups and study the formation of F8H2 gradients as a function of chemistries around the Si atom (methylchlorosilane vs trichlorosilane), the flux of the diffusing species, the type of diffusing medium (nitrogen vs humid air), and the nature of the substrate (continuous vs physically corrugated). To narrow the large set of parameters that affect the properties of the gradient surfaces, we fix some of the variables, such as the degree of confinement (all samples reported here were prepared by carrying out the gradient deposition in Petri dishes), the humidity (30−50%), and the temperature of the vapor medium and the substrate (both at ambient temperature). We develop correlations between the density of the F8H2 groups on the surface for a given end group type around the Si atom and the molecular orientation of the $-(CF_2)_8-$ mesogen. We also use the gradient geometry to study the mechanism of formation of semifluorinated SAMs from air and nitrogen gas and provide evidence that the presence of moisture in air leads to the formation of stable multimolecular complexes in trifunctional SFOs.

Experimental Section

Materials. 1*H*,1*H*,2*H*,2*H*-Perfluorodecyldimethylchlorosilane ($F(CF_2)_8(CH_2)_2Si(CH_3)_2Cl$, mF8H2) (CAS no. 74612-30-9) and 1*H*,1*H*,2*H*,2*H*-Perfluorodecyltrichlorosilane ($F(CF_2)_8(CH_2)_2SiCl_3$, tF8H2) (CAS no. 78560-44-8) were supplied by Lancaster and used as received. A Sylgard-184 poly(dimethylsiloxane) (PDMS) kit was purchased from Dow Chemical and applied according to the recipe specified by the manufacturer. Deionized (DI) water (resistivity > 16 MΩ·cm) was obtained using the Millipore water purification system. Single-side-polished, 300 mm thick silicon wafers with [100] orientation (Virginia Semiconductor, Inc.) were cut into ∼1 × 1, ∼1.5 × 1, or ∼1 × 5 cm^2 pieces, placed into an ultraviolet/ozone (UVO) cleaner (Jelight Co., model 42),[41] and exposed to UVO treatment for 30 min. This treatment produced a high concentration of the surface −OH groups at the silica surfaces that served as attachment points for the chlorosilane molecules.

(18) Daniel, S.; Chaudhury, M. K.; Chen, J. C. *Science* **2001**, *291*, 633. Daniel, S.; Chaudhury, M. K. *Langmuir* **2002**, *18*, 3404. Daniel, S.; Sircar, S.; Gliem, J.; Chaudhury, M. K. *Langmuir* **2004**, *20*, 4085.
(19) Petrie, R. J.; Bailey, T. N.; Gorman, C. B.; Genzer, J. *Langmuir* **2004**, *20*, 9893.
(20) Bhat, R. R.; Tomlinson, M. R.; Genzer, J. *J. Polym. Sci., Polym. Phys. Ed.* **2005**, *43*, 3384.
(21) Bhat, R. R.; Tomlinson, M. R.; Wu, T.; Genzer, J. Surface-Grafted Polymer Gradients: Formation, Characterization and Applications. *Adv. Polym. Sci.* **2006**, *198*, 51.
(22) Ionov, L.; Stamm, M.; Diez, S. *Nano Lett.* **2005**, *5*, 1910.
(23) Genzer, J. Molecular gradients: Formation and applications in soft condensed matter science. In *Encyclopedia of Materials Science*; Buschow, K. H. J., Cahn, R. W., Flemings, M. C., Ilschner, B., Kramer, E. J., Mahajan, S., Eds.; Elsevier: Oxford, 2002.
(24) Genzer, J.; Bhat, R. R.; Wu, T.; Efimenko, K. In *Molecular gradient nanoassemblies*; Nalwa, H. S., Ed.; American Scientific Publishers: Stevenson Ranch, CA, 2004.
(25) Genzer, J. *J. Adhes.* **2005**, *81*, 417.
(26) Geissler, M.; Xia, Y. N. *Adv. Mater.* **2004**, *16*, 1249.
(27) Roberson, S. V.; Fahey, A. J.; Sehgal, A.; Karim, A. *Appl. Surf. Sci.* **2002**, *200*, 150.
(28) Fosser, K. A.; Nuzzo, R. G. *Anal. Chem.* **2003**, *75*, 5775.
(29) Choi, S. H.; Zhang Newby, B. M. *Langmuir* **2003**, *19*, 7427.
(30) Morgenthaler, S.; Lee, S. W.; Zucher, S.; Spencer, N. D. *Langmuir* **2003**, *19*, 10459.
(31) Kraus, T.; Stutz, R.; Balmer, T. E.; Schmid, H.; Malaquin, L.; Spencer, N. D.; Wolf, H. *Langmuir* **2005**, *21*, 7796.
(32) Mougin, K.; Ham, A. S.; Lawrence, M. B. Fernadez, E. J.; Hillier, A. C. *Langmuir* **2005**, *21*, 4809.
(33) Sato, M.; Akimoto, K.; Takeuchi, A.; Suzuki, N.; Takasaki, Y.; Endo, A. *Kagaku Kogaku Ronbunshu* **2005**, *31*, 138.
(34) Geisler, M.; Chalsani, P.; Cameron, N. S.; Veres, T. *Small* **2006**, *2*, 760.
(35) Morgenthaler, S.; Lee, S. W.; Zucher, S.; Spencer, N. D. *Langmuir* **2006**, *22*, 2706.
(36) Venkataraman, N. V.; Zurcher, S.; Spencer, N. D. *Langmuir* **2006**, *22*, 4184.
(37) Wu, T.; Efimenko, K.; Genzer, J. *J. Am. Chem. Soc.* **2002**, *124*, 9394.
(38) Wu, T.; Efimenko, K.; Vlček, P.; Šubr, V.; Genzer, J. *Macromolecules* **2003**, *36*, 2448.
(39) Efimenko, K.; Fischer, D. A.; Douglas, J. F.; Phelan, F. R.; Genzer, J. Submitted for publication.
(40) Efimenko, K.; Fischer, D. A.; Douglas, J. F.; Genzer, J. Manuscript in preparation.
(41) Certain commercial equipment is identified in this paper to specify adequately the experimental procedure. In no case does such identification imply recommendation or endorsement by the National Institute of Standards and Technology, nor does it imply that the items identified are necessarily the best available for the purpose.

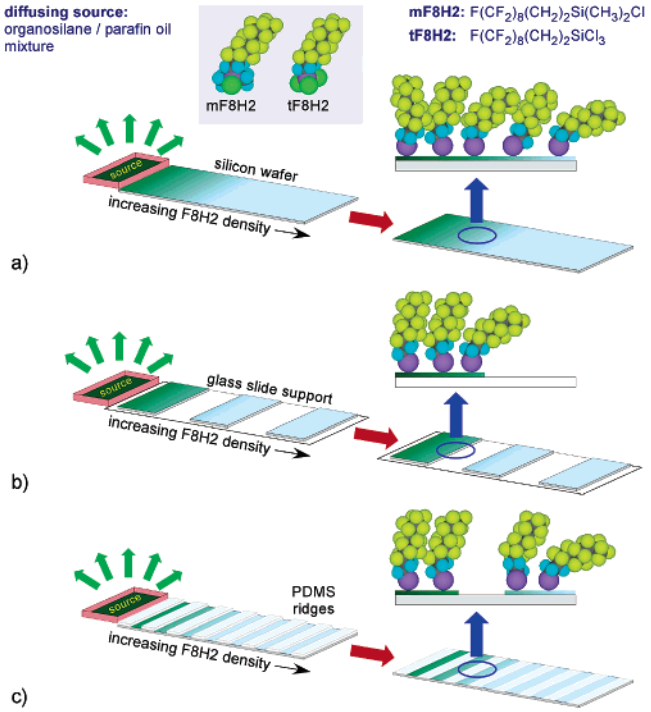

Figure 2. Schematic illustrating the formation of molecular gradients. A mixture of SFO and PO is placed into a small container and positioned at the edge of a flat substrate (see below). As the SF chlorosilane evaporates (the evaporation rate is regulated by the SFO:PO ratio), it creates a concentration gradient in the vapor phase, which then gets "imprinted" onto the substrate. The substrate can be (a) a flat continuous silicon wafer, (b) several small pieces of a flat silicon wafer, or (c) a silicon wafer covered with equidistantly spaced ridges made of PDMS network films (1 mm thick and ~5 mm wide). See the text for details of the individual substrates.

Formation of Molecular Gradients. The molecular gradients of mF8H2 and tF8H2 were formed by a variant of the method originally described by Chaudhury and Whitesides.[17] A small amount of SFO was mixed with paraffin oil (PO) in various ratios (see the text below for details) and placed into a small Teflon container. The flat silica-based substrate (specified below) was positioned horizontally next to the container, and the whole system was enclosed in a Petri dish (plastic or glass) and kept at ambient conditions. After a predetermined period of time the substrate was removed from the container, washed copiously with ethanol to remove any physisorbed organosilane molecules, and dried with nitrogen. We have deposited SFO gradients on three types of surfaces. The first type involved plain silicon wafers (~1 × 5 cm^2) with surface-bound hydroxyl groups (cf. Figure 2a). The second substrate type was made by placing smaller pieces of silicon wafers (~1 × 1 or ~1.5 × 1 cm^2) onto a glass substrate such that there were "gaps" between two adjacent silicon pieces (cf. Figure 2b). Finally, we have performed experiments on silica wafer substrates decorated with equidistantly spaced PDMS ridges (cf. Figure 2c). The latter kind of substrate was fabricated by first depositing a fixed amount of a mixture of PDMS chains and a cross-linker onto plain silicon wafers (~1 × 5 cm^2) and curing them at 55 °C for about 1 h to form PDMS networks. The amount of PDMS was adjusted such that the height of the PDMS ridges on the substrate was always 1.5 mm. Using a scalpel, we cut ridges into the cured PDMS film (parallel to the shorter side of the substrate) and peeled off alternating PDMS pieces from the substrate. No residues of PDMS on the peeled areas were found (confirmed by NEXAFS measurements discussed further below). UVO treatment was used to clean the exposed parts of the silicon wafers and to generate surface-bound hydroxyls needed for SFO attachment. After gradient deposition, the remaining PDMS ridges on the substrates were removed by being peeling off before gradient analysis.

Experimental Techniques. Contact angle experiments were carried out using a Ramé-Hart contact angle goniometer, model 100-00. A small droplet (~4 μL) of deionized water (resistivity >16 MΩ·m) was deposited onto the surface and kept in contact with the needle. The advancing contact angle was read at the front position of the droplet. The receding contact angles were also determined by reading the wettability at the receding edge of the droplet. Only advancing contact angles are reported here; the contact angle hysteresis was ranging from 10 to 25°. Each data point reported in the paper represents an average over three measurements, each measured on a fresh portion of the sample.

We used near-edge X-ray absorption fine structure (NEXAFS)[42,43] spectroscopy to determine the concentration of the F8H2 groups and their molecular orientation on the surface. The NEXAFS experiments were carried out in the NIST/Dow Soft X-ray Materials Characterization Facility at the National Synchrotron Light Source at Brookhaven National Laboratory (NSLS BNL).[44] NEXAFS spectroscopy involves the resonant soft X-ray excitation of a K- or L-shell electron to an unoccupied low-lying antibonding molecular orbital of σ symmetry, σ^*, or π symmetry, π^*.[42] The initial-state K-shell excitation gives NEXAFS its element specificity, while the final-state unoccupied molecular orbitals provide NEXAFS with its bonding or chemical selectivity. A measurement of the partial electron yield (PEY) intensity of NEXAFS spectral features thus allows for the identification of chemical bonds and determination of their relative population density within the sample. Moreover, by collecting the PEY NEXAFS spectra at several sample geometries defined by θ ($20° \leq \theta \leq 90°$), the angle between the sample normal and the polarization vector of the X-ray beam, the average surface molecular orientation of the F8H2 SAM molecules on the silicon oxide surfaces can be determined. An important issue concerning the study of organic materials is the possibility of sample damage during the characterization with UV light and X-ray and electron radiation. Semifluorinated materials are particularly sensitive to these effects.[45] The data collection scheme implemented in this work minimized any damage to the same due to the X-ray exposure. Specifically, the information about the concentration of F8H2 moieties on the surfaces was obtained via combinatorial NEXAFS (combi-NEXAFS) methodology,[46] which is based on monitoring the PEY intensity while simultaneously rastering the sample across the X-ray beam. The typical raster step implemented in this work was 0.5 mm. The PEY signal was collected at $\theta = 50°$, which is close to the "magic angle",[42] a geometry in which the signal is independent of the molecular orientation. In addition, we performed experiments at $\theta = 20°$ and 90°. By combining the data collected at all three angles, we could determine the average molecular orientation of the $-(CF_2)_8-$ mesogens on the surface.[47−49] The PEY signals were collected for both carbon and fluorine K-edges at incident X-ray energies of 280 eV (carbon K-edge) or 680 eV (fluorine K-edge) for the preedge, 292 eV (carbon K-edge) or 692 eV (fluorine K-edge) for the $1s \rightarrow \sigma^*_{C-F}$ signal, and 320 eV (carbon K-edge) or 720 eV (fluorine K-edge) for the postedge. The resultant PEY NEXAFS signals were normalized by following the methodology outlined by Outka and

(42) Stöhr, J. *NEXAFS Spectroscopy*; Springer-Verlag: Berlin, 1992.
(43) See for example: Zharnikov, M.; et al. *Phys. Chem. Chem. Phys.* **2000**, *2*, 3359. Frey, S.; et al. *Isr. J. Chem.* **2000**, *40*, 81. Bagus, P. S.; et al. *Chem. Phys. Lett.* **1996**, *248* 129.
(44) For detailed information about the NIST/Dow Soft X-ray Materials Characterization Facility at NSLS BNL, see: http://nslsweb.nsls.bnl.gov/nsls/pubs/newsletters/96-nov.pdf.
(45) Jäger, B.; et al. *Phys. Chem.* **1997**, *202*, 263. Wirde, M.; et al. *Nucl. Instrum. Methods Phys. Res., B* **1997**, *131*, 245. Zharnikov, M.; et al. *Phys. Chem. Chem. Phys.* **1999**, *1*, 3163.
(46) Genzer, J.; Fischer, D. A.; Efimenko, K. *Appl. Phys. Lett.* **2003**, *82*, 266.
(47) Genzer, J.; Sivaniah, E.; Kramer, E. J.; Wang, J.; Körner, H.; Xiang, M.; Char, K.; Ober, C. K.; DeKoven, B. M.; Bubeck, R. A.; Chaudhury, M. K.; Sambasivan, S.; Fischer, D. A. *Macromolecules* **2000**, *33*, 1882.
(48) Genzer, J.; Sivaniah, E.; Kramer, E. J.; Wang, J.; Xiang, M.; Char, K.; Ober, C. K.; Bubeck, R. A.; Fischer, D. A.; Graupe, M.; Colorado, R., Jr.; Shmakova, O. E.; Lee, T. R. *Macromolecules* **2000**, *33*, 6068.
(49) Genzer, J.; Kramer. E. J.; Fischer, D. A. *J. Appl. Phys.* **2002**, *92*, 7070.

co-workers,[50] namely, by subtracting the preedge signal from the 1s $\rightarrow \sigma^*_{C-F}$ signal and scaling the postedge to 1 for each spot on the specimen. To convert the normalized PEY NEXAFS signals into concentrations of molecules, we have prepared densely packed SAMs from each organosilane, collected PEY NEXAFS spectra,[51] and used them to normalize the PEY NEXAFS spectra in the gradient samples. Considering that the PEY intensity at $\theta = 50°$ is directly proportional to the concentration of the molecules, such $PEY_{gradient}/PEY_{SAM}$ intensity maps have a unit of a fraction of F8H2 molecules in the SAM.

Results and Discussion

Initial studies of wettability gradients relied primarily on contact angle measurements.[10] Despite their simplicity, wettability measurements can deliver very useful information not only about the chemical nature of the substrates but also about their degree of uniformity. Unfortunately, there are some downsides associated with measuring wettabilities on gradient substrates. If one wants to gain knowledge about the surface energetic locally along the gradient, one needs to use relatively small volumes of the probing liquid. Because of the wettability gradient, free droplets would move along the gradient and not be held in space. Therefore, to immobilize the drop at a given position on the substrate, the droplet needs to remain in contact with the needle at all times. The obstacles can in principle be circumvented by using larger droplets and moving them along the substrate with the needle. The advancing and receding contact angle values can be determined as a function of the position of the front and the back of the drop, respectively. One complication may still be encountered that stems from distorting the droplet shape due to the nonequal wettabilities at the front and back of the droplet. We have recently shown that combi-NEXAFS provides a convenient complementary means of probing the characteristics of wettability gradients.[46] Specifically, by monitoring the chemical signal originating from a specific part of the molecule (in the case of the SFO, the fluorine signal) and rastering the X-ray beam across the sample, one can unambiguously establish the spatial distribution of the adsorbed molecules in the molecular gradient. A second advantage of combi-NEXAFS is that it can simultaneously probe both the concentration and the orientation of the adsorbed molecules on the substrate. To achieve the latter, NEXAFS scans measured at various sample-to-beam orientations are needed. We will return to this point later in the paper when we discuss our method of measuring the orientation of SFOs in the molecular gradients.

To illustrate the principles of determining the concentration of SFO in molecular gradients using NEXAFS, we first show NEXAFS spectra in tF8H2 homogeneous SAMs. In Figure 3 we plot the partial yield (PEY) NEXAFS signal as a function of the photon energy around the carbon K-edge collected at three different sample geometries. There are several peaks present in the NEXAFS spectra; the most prominent are those at 292 and 295 eV, which correspond to the 1s $\rightarrow \sigma^*$ transitions of the C−F and C−C bonds, respectively.[46−49] We use these two signals to monitor the concentration and orientation of the F8H2 moieties on the surfaces. The height of each peak bears two kinds of information. First, it is the concentration of the molecules on the surface that determines the number of generated Auger electrons that contribute to the PEY NEXAFS signal. Second, as apparent from the data in Figure 3, also the orientation of the antibonding (σ^*) orbitals with respect to the electric vector of the polarized

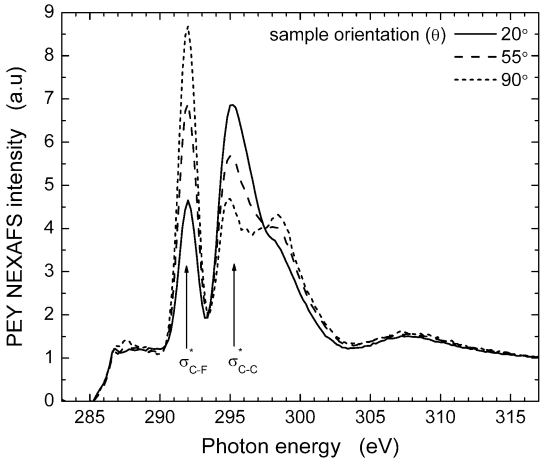

Figure 3. Partial electron yield carbon K-edge NEXAFS spectra collected from a homogeneous tF8H2 SAM deposited on silica substrates. The spectra were recorded at angles between the electric vector of the X-ray beam and the sample normal (θ) equal to 20° (solid line), 50° (dashed line), and 90° (dotted line).

X-ray beam influences the intensity of the 1s $\rightarrow \sigma^*$ transition signals. Considering that σ^* orbitals are aligned along the σ bonds of the respective C−F and C−C bonds and recognizing that in the spectra in Figure 3 an increase in the 1s $\rightarrow \sigma^*_{C-F}$ intensity with varying the sample orientation with respect to the X-ray beam is accompanied by a decrease in the 1s $\rightarrow \sigma^*_{C-C}$ intensity, the data reveal that, in F8H2 molecules, the C−F and C−C bonds are oriented roughly perpendicularly to one another. A more involved analysis can be invoked[49] to determine the actual F8H2 orientation on the sample. The spectra collected at $\theta = 50°$ are important as at this geometry the measurement is almost insensitive to the molecular orientation;[42,46−49] hence, NEXAFS data recorded at $\theta = 50°$ provide a convenient measure of the concentration of the F8H2 molecules on the surface. In previous papers we have demonstrated that, by collecting NEXAFS spectra, such as the one shown in Figure 3, as a function of the position on the substrate, one can gather information about the in-plane concentration and molecular orientation.[47−49] We have also shown that to accomplish this one does not always need to collect the entire spectrum; monitoring the PEY around the C−F and C−C peaks is sufficient to learn about the molecular orientation in SFOs.

Information obtained from combi-NEXFAS can be compared with the wettability measurements. In Figure 4 we plot the negative cosine of the contact angle (left ordinate, discrete points) values of deionized water collected from a wettability gradient prepared by diffusing tF8H2 from tF8H2:PO = 1:1 (w/w) mixtures for various times in air. In the same figure we also plot the concentration profiles of F8H2 in the molecular gradients determined by combi-NEXFAS in the same sample (right ordinate, lines). The agreement between the two methods is excellent. In our further discussion in this paper we will thus rely solely on the NEXAFS data.

Taking advantage of NEXAFS's ability to determine the molecular orientation on surfaces, for each sample we monitored the 1s $\rightarrow \sigma^*$ PEY NEXAFS for both C−F and C−C bonds at three different orientations. In Figure 5 we plot the maxima of the 1s $\rightarrow \sigma^*_{C-F}$ and 1s $\rightarrow \sigma^*_{C-C}$ signals collected at $\theta =$ (a) 20°, (b) 50°, and (c) 90° as a function of the position on the sample comprising a tF8H2 molecular gradient deposited from tF8H2:PO = 1:1 (w/w) mixtures diffusing for 10 min in air. Note that the PEY NEXAFS values for both C−F and C−C signals at all angles in the gradient sample near the diffusing source (low

(50) Outka, D. A.; Stöhr, J.; Rabe, J. P.; Swalen, J. D.; Rotermnd, H. H. *Phys. Rev. Lett.* **1987**, *59*, 1321. Outka, D.; Stöhr, J.; Rabe, J.; Swalen, J. D. *J. Chem. Phys.* **1988**, *88*, 4076.

(51) Genzer, J.; Efimenko, K.; Fischer, D. A. *Langmuir* **2002**, *18*, 9307.

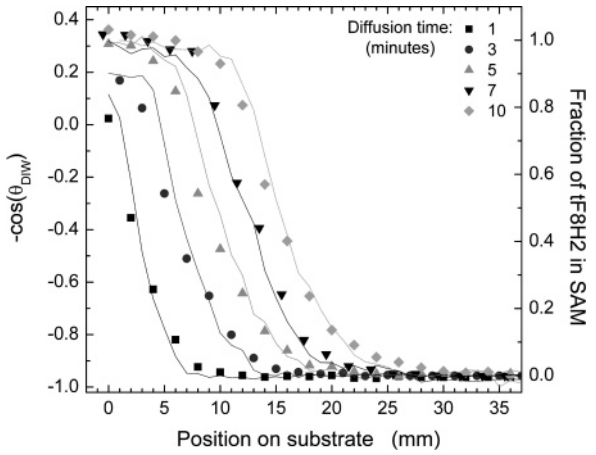

Figure 4. Negative cosine of the contact angle measured with DI water (left ordinate, symbols) and the fraction of tF8H2 in a gradient SAM determined by combinatorial NEXAFS spectroscopy (right ordinate, lines) from tF8H2 gradients prepared by diffusion of tF8H2:PO = 1:1 (w/w) mixtures for 1 (squares), 3 (circles), 5 (up-triangles), 7 (down-triangles), and 10 (tilted squares) min.

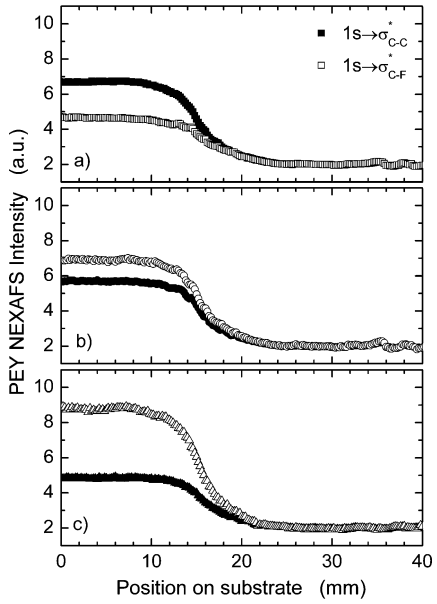

Figure 5. Maxima of the 1s → σ^*_{C-F} (solid symbols) and 1s → σ^*_{C-F} (open symbols) signals in the partial electron yield NEXAFS spectra collected at energies of 292 and 295 eV, respectively, and at θ = (a) 20° (squares), (b) 50° (circles), and (c) 90° (up-triangles) from tF8H2 gradient samples deposited from tF8H2:PO = 1:1 (w/w) mixtures for 10 min in air.

value on the abscissa) are close to the corresponding PEY NEXAFS intensity signals measured on a homogeneous tF8H2 SAM (cf. Figure 3). This indicates that the F8H2 SAM close to the diffusing source has a coverage corresponding roughly to the homogeneous SAM. As one traverses across the sample (position coordinate in the data in Figure 5), 1s → σ^*_{C-F} and 1s → σ^*_{C-C} start to decrease (~12 mm) and eventually drop to a small constant value (>24 mm). The coordinates between 12 and 24 mm positions depict the region on the sample where the molecular gradient of F8H2 is located. As mentioned earlier, at θ = 50° the PEY NEXAFS data are not affected by the SFO molecular orientation; hence, they provide a measure of the concentration of F8H2 in the gradient. When combined with the data collected at the two remaining angles, one can translate the PEY NEXAFS intensities into the orientation of the F8 group on the substrate. We express this orientation in terms of the so-called average tilt

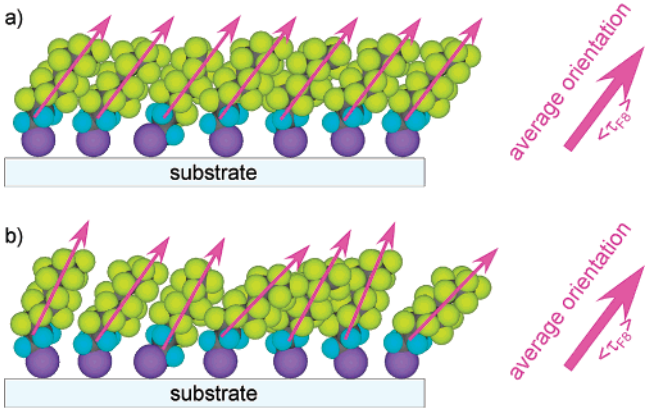

Figure 6. Schematics depicting the organization of F8H2 molecules on substrates with the F8 mesogens pointing in the same direction (a) and those in which they point "on average" in one direction (b). In both cases, the average molecular orientations of the F8 mesogen, $\langle\tau_{F8}\rangle$, are the same.

angle of the $-(CF_2)_8F$ group, $\langle\tau_{F8}\rangle$. Considering that the spot size of the X-ray beam on the sample during the NEXAFS experiments, ~1 mm^2, is much larger than the area occupied by a single tF8H2 molecule, the tilt angle $\langle\tau_{F8}\rangle$ determined from NEXAFS represents only an *average* value. Hence, there is no straightforward way to discriminate between the case of all tF8H2 molecules being homogeneously tilted by the same angle and the case of a disordered system with a broad distribution of tilt angles pointing in one average direction (cf. Figure 6). Therefore, the variation in $\langle\tau_{F8}\rangle$ observed in the region of the gradient (see below) in which the concentration decreases cannot be unambiguously interpreted by using the NEXAFS data alone. Complementary measurement of another physical property along the gradient, such as the density and/or the thickness, is required. Nevertheless, we still use $\langle\tau_{F8}\rangle$ as a convenient means of characterizing the molecular orientation of SFOs on the surface.

Using all three angles and by utilizing previously developed analysis methods,[49] we convert the position-dependent PEY NEXAFS data into $\langle\tau_{F8}\rangle$ in the gradient. In Figure 7 we plot the concentration of F8H2 (in terms of the fraction of tF8H2 in homogeneous SAMs) (left ordinate, solid symbols) and the corresponding values of $\langle\tau_{F8}\rangle$ (right ordinate, open symbols) as a function of the position on the substrate for samples prepared by diffusing tF8H2:PO = 1:1 (w/w) mixtures for (a) 3, (b) 5, and (c) 7 min. In all instances, the concentration of F8H2 starts high, decreases as one moves across the gradient region, and finally reaches zero, where no F8H2 species can be found. The concentration of F8H2 in the sample region near the diffusing source is high, but at short diffusion times it still does not achieve a coverage measured in a homogeneous tF8H2 SAM. Only after ~10 min, the fraction of tF8H2 in the gradient sample matches that in the homogeneous SAM. By exploring $\langle\tau_{F8}\rangle$ in the plots in Figure 7, one can see that in the densely packed regions in the sample, the F8H2 molecules stand almost perpendicular to the sample surface. Across the gradient region, the average orientation of the $-(CF_2)_8-$ mesogens changes; they start to tilt and finally become completely disoriented (very randomly oriented) at the very edge of the sample, where there is only a very small concentration of the F8H2 groups on the surface. By comparing the profiles of the F8H2 concentration and $\langle\tau_{F8}\rangle$ within the gradient, we can see that the latter drops more sharply, indicating that either the F8H2 molecules tilt more rapidly or they become more and more disorganized. Recalling that $\langle\tau_{F8}\rangle$

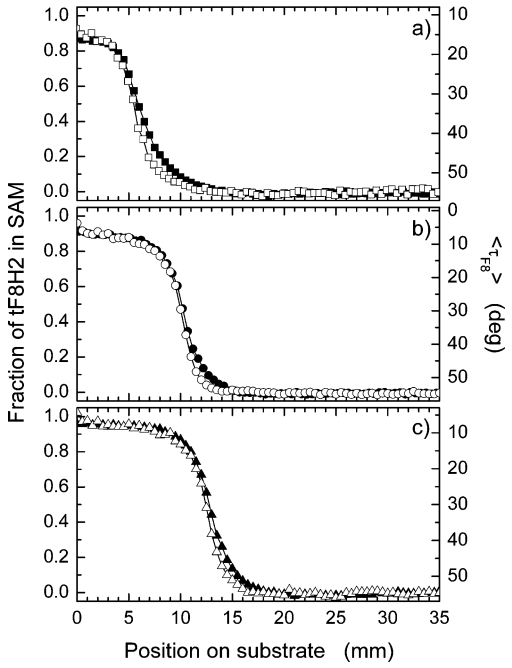

Figure 7. Fraction of tF8H2 in a gradient SAM (left ordinate, solid symbols) and the corresponding average molecular orientation of the F8 mesogen, $\langle\tau_{F8}\rangle$ (right ordinate, open symbols), as a function of the position on the substrate for samples prepared by diffusing tF8H2:PO = 1:1 (w/w) mixtures for (a) 3, (b) 5, and (c) 7 min.

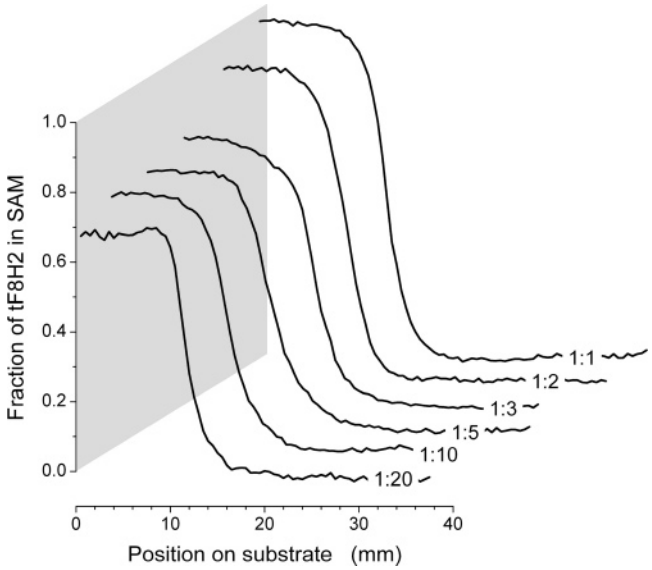

Figure 8. Fraction of tF8H2 in a gradient SAM as a function of the position on the substrate for samples prepared by diffusing tF8H2:PO mixtures of various concentrations (w/w) ranging from 1:1 to 1:20 for 7 min.

represents only an average orientation of the sample population probed by NEXAFS, the latter explanation seems to be more feasible.

In their original paper, Chaudhury and Whitesides pointed out that the flux of the organosilanes diffusing from the source can be conveniently adjusted by premixing the silane with PO. In our experiments we have explored a whole range of SFO:PO compositions ranging from 1:1 to 1:20 (w/w). The effect of diluting SFOs with PO on the concentration profiles of F8H2 is demonstrated by the data shown in Figure 8, where we plot the concentration of tF8H2 in the molecular gradient as a function of the position on the sample, which was prepared by evaporating tF8H2 from SFO:PO mixtures of varying concentrations for 7 min in air. From the data in Figure 8 it becomes apparent that the dilution affects primarily the amount of F8H2 species incorporated into the substrate, not the diffusing length, as expected. The aforementioned concentration effects are not that large, however. This may be due to the chemical incompatibility between SFO and PO, which would lead to local phase separation in the diffusing source. Having a lower surface energy than PO, SFO will segregate to the surface and will hence be present in larger quantities relative to the case of a fully homogeneous mixture. A possible drawback of using PO as a diluent may be associated with the formation of SFO networks—in cases where air is used as a diffusing medium and SFO is equipped with a trichlorosilane group (this will not happen when only monofunctionalized chlorosilanes are used). The phase separation in the diffusing source combined with the presence of a small amount of moisture around the diffusing source may thus lead to local cross-linking among neighboring SFO molecules, resulting in the formation of a siloxane network. Initially, we noted that these networks formed when we let such a diffusing source sit in air for 20 min and longer. To circumvent this problem, we have designed a simple mixing device powered by a magnet that allows us to constantly mix the content of the diffusing source during the gradient formation and disperse the SFO and PO in the source. The mixing is very slow; it has no effect on the properties of the gradients.

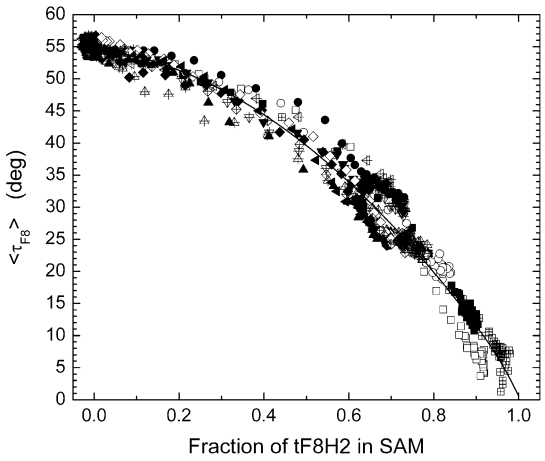

Figure 9. Average tilt angle of the F8 mesogen, $\langle\tau_{F8}\rangle$, in a tF8H2 SAM as a function of the fraction of tF8H2 in the SAM, f_{tF8H2}, for tF8H2:PO (w/w) mixtures equal to 1:1 (squares), 1:2 (circles), 1:3 (up-triangles), 1:5 (down-triangles), 1:10 (tilted squares), and 1:20 (left triangles) diffusing in air for 3 (solid symbols), 5 (open symbols), and 7 (crossed symbols) min. The line represents the best fit to the data using the second-order polynomial $\langle\tau_{F8}\rangle = 54.75647 - 7.9208 f_{tF8H2} - 44.53841 f_{tF8H2}^2$.

Using the data collected at various SFO/PO concentrations and evaporation times, we can establish a correlation between the average tilt angle of the fluorinated part of the F8H2 mesogen, $\langle\tau_{F8}\rangle$, and the concentration of tF8H2 in the gradient. In Figures 9 and 10 we plot $\langle\tau_{F8}\rangle$ as a function of the fraction of tF8H2 in the gradient for molecular gradients, f_{tF8H2}, formed in air and in nitrogen gas, respectively. As apparent from the plots, all data collapse onto unique master plots. Hence, there is a direct correlation between $\langle\tau_{F8}\rangle$ and f_{tF8H2}. We fit the correlations to a second-order polynomial; the best fits are provided in the captions to Figures 9 and 10.

We have also studied the formation of molecular gradients made of monofunctionalized SFOs, mF8H2. The normal boiling point of mF8H2 is lower (198 °C) than that of tF8H2 (224 °C). Hence, mF8H2 would evaporate even more readily at ambient conditions. The gradients were formed by following the same

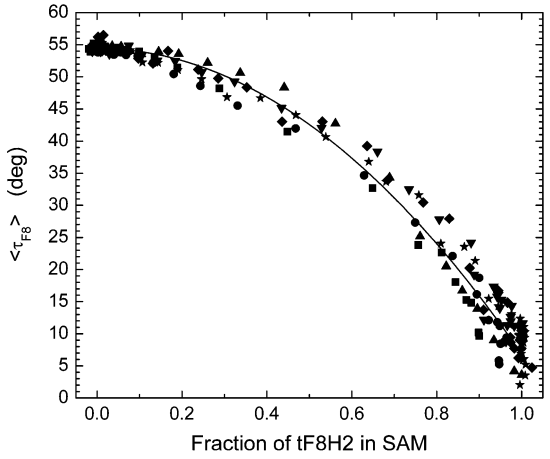

Figure 10. Average tilt angle of the F8 mesogen, $\langle\tau_{F8}\rangle$, in a tF8H2 SAM as a function of the fraction of tF8H2 in the SAM, f_{tF8H2}, for tF8H2:PO (w/w) mixtures equal to 1:5 diffusing in nitrogen for 3 (squares), 5 (circles), 7 (up-triangles), 10 (down-triangles), 15 (tilted squares), and 20 (stars) min. The line represents the best fit to the data using the second-order polynomial $\langle\tau_{F8}\rangle = 54.40486 + 0.27216f_{tF8H2} - 47.84104f_{tF8H2}^2$.

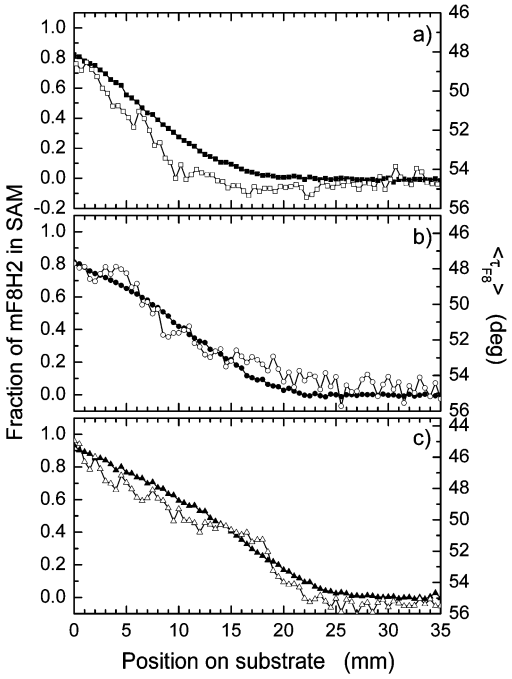

Figure 11. Fraction of mF8H2 in a SAM (left ordinate, solid symbols) and the corresponding average molecular orientation of the F8 mesogen, $\langle\tau_{F8}\rangle$ (right ordinate, open symbols), as a function of the position on the substrate for samples prepared by diffusing mF8H2:PO = 1:1 (w/w) mixtures for (a) 3, (b) 5, and (c) 7 min.

procedure as described earlier for tF8H2; their properties were studied using combi-NEXAFS. In Figure 11 we plot the fraction of mF8H2 in the gradient SAM (left ordinate, solid symbols) and $\langle\tau_{F8}\rangle$ (right ordinate, open symbols) for gradient samples prepared by evaporating mF8H2 from mF8H2:PO = 1:1 (w/w) mixtures for (a) 3, (b) 5, and (c) 7 min. As previously discussed for the tF8H2 gradients, the concentration of mF8H2 in the SFO molecular gradient changes gradually across the sample. However, relative to the gradient profiles measured in tF8H2 specimens (cf. Figure 7), the spatial variation of density and molecular orientation in mF8H2 gradients is much shallower. Hence, it is apparent that the functional dependence of the concentration profiles is governed by the type of molecular bonding on the

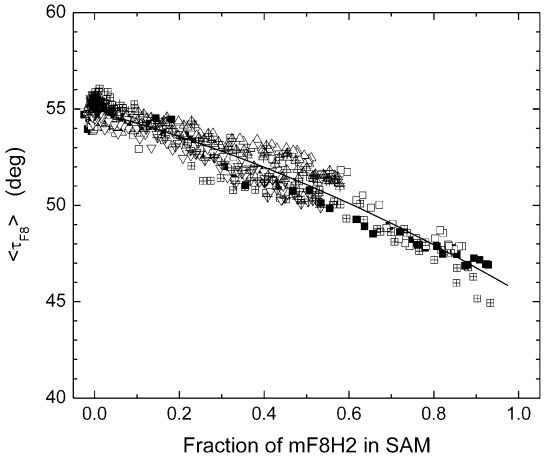

Figure 12. Average molecular orientation of the F8 mesogen, $\langle\tau_{F8}\rangle$, in an mF8H2 SAM as a function of the fraction of mF8H2 in the SAM, f_{mF8H2}, for mF8H2:PO (w/w) mixtures equal to 1:1 (squares), 1:2 (circles), 1:3 (up-triangles), 1:5 (down-triangles), 1:10 (tilted squares), and 1:20 (left triangles) diffusing for 3 (solid symbols), 5 (open symbols), and 7 (crossed symbols) min. The line represents the best fit to the data using the second-order polynomial $\langle\tau_{F8}\rangle = 54.884 - 5.83157f_{mF8H2} - 3.54485f_{mF8H2}^2$.

substrate. This can be due to several factors. First, unlike the monofunctional mF8H2 molecules, the tF8H2 species have a tendency to form larger multimolecular clusters. This behavior has been known for some time and is relatively well-documented.[52] These clusters can form either in the vapor phase or/and after the molecules land on the silica surface. Thus, unlike the mF8H2 SAMs, which are formed primarily by deposition of single molecules, the tF8H2 SAMs may be built by inserting clusters containing multiple molecules. We will return to the discussion about clusters later in the paper. The second factor, which is closely associated with the first one, has to do with the way the F8H2 organosilanes pack. We have recently reported that the orientation of the F8H2 molecules in homogeneous SAMs depends on the bonding environment of the F8H2 molecule. The average tilt angles of the semifluorinated part of tF8H2 and mF8H2 moieties from the surface normal, $\langle\tau_{F8}\rangle$, were $10 \pm 2°$ and $45 \pm 3°$, respectively.[51] The increase of the average tilt angle with increasing number of methyl groups attached to the silicon terminus was associated with the steric hindrance of those methyl groups close to the bonding substrate.[51] The data in Figure 11 reveal that $\langle\tau_{F8}\rangle$ values in mF8H2 gradients also vary as a function of the position on the sample; they decrease as the concentration of mF8H2 on the substrate decreases. Similarly to the previous data treatment presented for the tF8H2 gradients, we find correlations between $\langle\tau_{F8}\rangle$ and the fraction of mF8H2 in the gradient for molecular gradients, f_{mF8H2}, formed in air. In Figure 12 we plot $\langle\tau_{F8}\rangle$ as a function of f_{mF8H2} for gradient samples prepared by diffusing mF8H2 from SFO/PO mixtures of various concentrations in air. The best fit to a second-order polynomial is listed in the caption to Figure 12.

In the Introduction, we have postulated that the gradient geometry facilitates a convenient means of studying the mechanism of formation of SAMs. In contrast to the generation of homogeneous SAMs, where all molecules impinge on the substrate in a "homogeneous" manner, in gradient geometries, the SAM-forming moieties get incorporated in a directional manner. In the remainder of this paper we describe two kinds

(52) Banga, R.; Yarwood, J.; Morgan, A. M.; Evans, B.; Kells, J. *Langmuir* **1995**, *11*, 4393. Bunker, B. C.; Carpick, R. W.; Assink, R. A.; Thomas, M. L.; Hankins, M. G.; Voight, J. A.; Sipola, D.; de Boer, M. P.; Gulley, G. L. *Langmuir* **2000**, *16*, 7742.

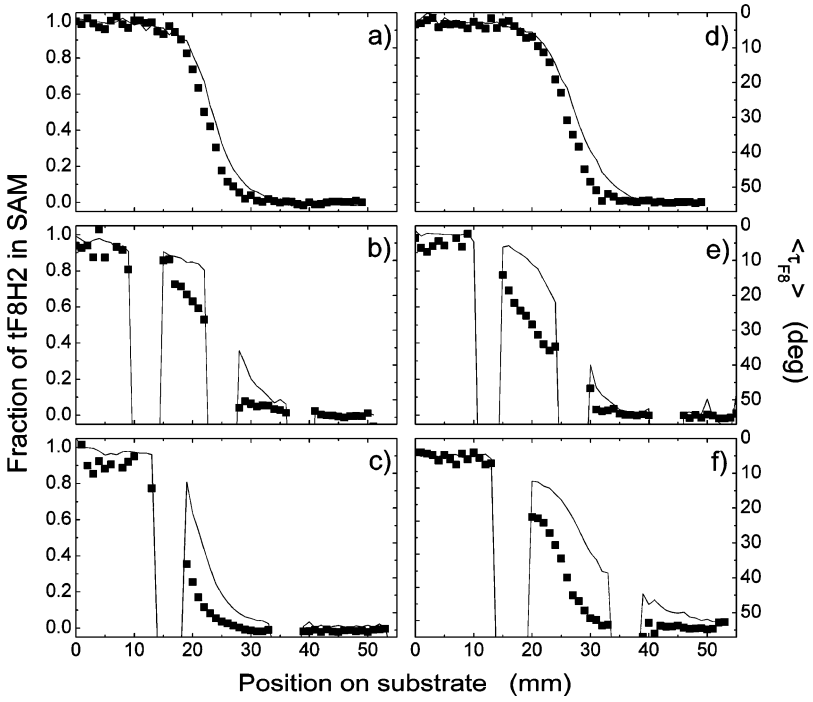

Figure 13. Fraction of tF8H2 in a tF8H2 gradient (left ordinate, solid line) and average orientation of the F8 mesogen, $\langle\tau_{F8}\rangle$ (right ordinate, solid points), in a molecular gradient prepared by diffusion from tF8H2:PO = 1:1 (w/w) mixtures in air for 15 min (a−c) and 20 min (d−f). The gradients were deposited into a continuous silicon wafer (a, d) and on a substrate comprising a silicon wafer cut into pieces 1 cm (b, e) and 1.5 cm (c, f) long. See Figure 2 and the text for the methodology.

of experiments utilizing gradient geometry, which we believe provide practical insight into the mechanism governing the formation of SFO SAMs. In both cases, we modify the nature of the substrates, such that we no longer work only with flat continuous silicon wafers.

In the first set of experiments, we cut the substrates into smaller pieces and separate them via gaps (for details see the Experimental Section and Figure 2b). The discontinuous silicon wafer pieces are mounted on top of a glass slide, and the gradient of tF8H2 is formed as previously discussed. After gradient formation, the samples are removed from the glass slide and analyzed via combi-NEXAFS. In Figure 13 we plot the fraction of tF8H2 in the gradient (left ordinate, solid line) and the average orientation of the F8 mesogen, $\langle\tau_{F8}\rangle$ (right ordinate, solid points), in the tF8H2 molecular gradient prepared by evaporation of tF8H2 from tF8H2:PO = 1:1 (w/w) mixtures in air for 15 min (a−c) and 20 min (d−f). Parts a and d denote samples prepared on continuous substrates; the remaining parts of the figure represent data collected from samples formed on discontinuous gradients. The sizes of the discontinuous pieces were ∼1 cm (b, e) and ∼1.5 cm (c, f). By exploring the concentration of tF8H2 molecules in all cases, the diffusion profiles on the continuous and discontinuous samples exhibit similar lengths and broadnesses. This behavior suggests that the transportation of molecules in the vapor phase is the dominant factor governing the formation of molecular gradients. This finding is perhaps not that surprising given the rather high diffusivity of tF8H2 in air, 6×10^{-4} cm^2/s, as measured earlier.[39] What is surprising, however, is the behavior of $\langle\tau_{F8}\rangle$. While close to the diffusing source the average molecular orientation of the F8H2 groups is the same on both the continuous and discontinuous substrates, $\langle\tau_{F8}\rangle$ on the discontinuous substrates after at least one discontinuity gap does not follow the trend seen in the continuous sample. From the data in Figure 13 it seems as if when encountering a new sample edge right after the discontinuity the F8H2 molecules lose "orientation memory" set out by the already formed SAM. Specifically, at the beginning of each new edge, the molecular orientation in the discontinuous samples is "worse" than that in the continuous specimens. This behavior suggests that molecules get incorporated into the SAM in a way that is dictated strongly by their neighbors. When a molecule "sees" an already-organized molecular pattern, it follows it readily. In contrast, when a new pattern has to be created with no "molecular seeds" present, such as at the edges of each new silicon sample, the memory of the previous orientation is lost. We note that although only data for two different diffusion times are shown here, this behavior has been seen consistently for many diffusion times.

In the second set of experiments we utilize specimens fabricated by using the method depicted in Figure 2c. Specifically, we create small diffusion barriers made of PDMS networks on flat silica substrates to confine both the motion of the molecules along the substrates and the deposition of the molecules from the vapor phase (the PDMS ridges act as additional diffusion barriers). In Figures 14 and 15 we plot the concentration of (a) mF8H2 molecules in mF8H2 gradients deposited in air, (b) tF8H2 molecules in tF8H2 gradients deposited in air, and (c) tF8H2 molecules in tF8H2 gradients deposited in nitrogen gas after evaporation for 10 and 20 min, respectively. In both figures we show the concentration of F8H2 in gradients formed on continuous substrates (solid symbols) and that measured on the PDMS-ridge-covered samples (open symbols). As expected the concentration profiles of both SFOs on the continuous substrates extend over larger distances from the diffusing source relative to those measured on the structured substrates. Also, as previously noted the concentration profiles of mF8H2 are broader than those of tF8H2 specimens. There are interesting trends seen in the formation of F8H2 gradients on the substrates decorated with PDMS ridges. To better understand their behavior, we superimpose approximated diffusion profiles for the case of the diffusion across the PDMS ridges (dotted lines in Figures 14 and 15). These lines provide guidance for a relative comparison among the various profiles. Also in Figures 14 and 15, with arrows we

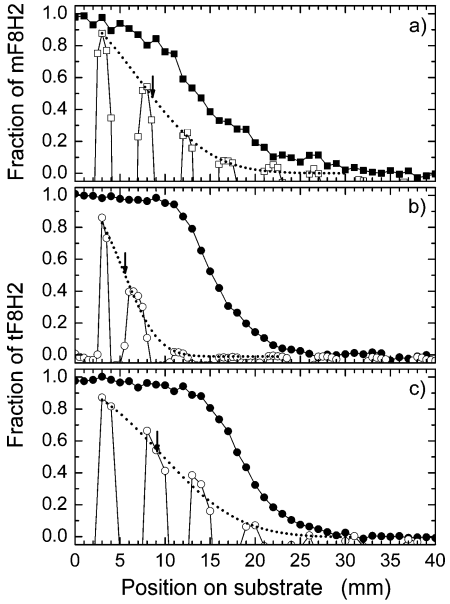

Figure 14. Fraction of mF8H2 (squares) in an mF8H2 molecular gradient prepared by diffusion from mF8H2:PO = 1:1 (w/w) mixtures in air (a). Fraction of tF8H2 (circles) in a tF8H2 gradient prepared by diffusion of tF8H2:PO = 1:1 mixtures in air (b) and in nitrogen (c). In all cases, the diffusion process took 10 min. The diffusion was carried out across a flat silica substrate (closed symbols) or across a flat silica substrate with PDMS ridges (open symbols); see the text for details. The dotted lines denote the approximated diffusion profiles for the case of the diffusion across the PDMS ridges. The arrows mark the positions on the diffusion front.

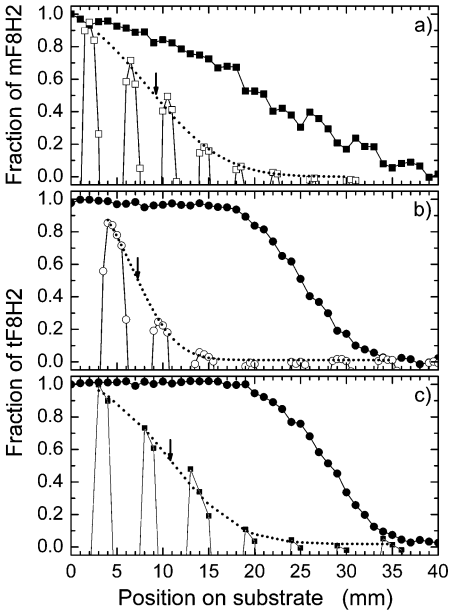

Figure 15. Fraction of mF8H2 (squares) in an mF8H2 molecular gradient prepared by diffusion from mF8H2:PO = 1:1 mixtures in air (a). Fraction of tF8H2 (circles) in a tF8H2 gradient prepared by diffusion of tF8H2:PO = 1:1 (w/w) mixtures in air (b) and in nitrogen (c). In all cases, the diffusion process took 20 min. The diffusion was carried out across a flat silica substrate (closed symbols) or across a flat silica substrate with PDMS ridges (open symbols); see the text for details. The dotted lines denote the approximated diffusion profiles for the case of the diffusion across the PDMS ridges. The arrows mark the positions on the diffusion front.

mark the position of the diffusing front for the concentration on the substrates containing the PDMS barriers. What is clear from the data in both figures is the fact that the position of the diffusing

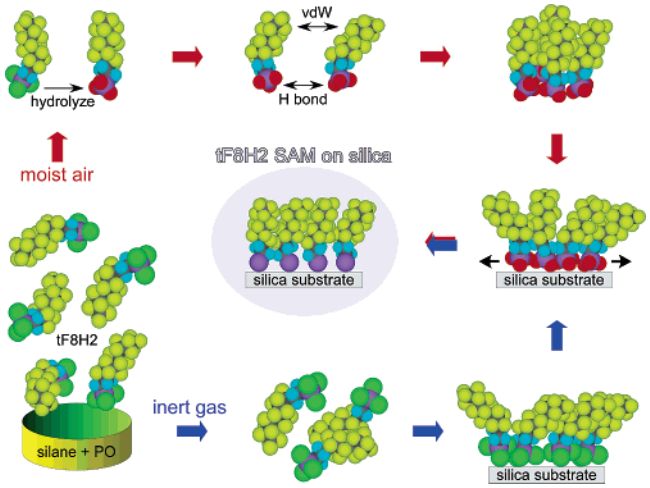

Figure 16. Schematic illustrating the proposed pathway leading toward the formation of self-assembled monolayes of tF8H2 in air (top path, red arrows) and nitrogen (bottom part, blue arrows).

fronts for mF8H2 (a) and tF8H2 deposited in nitrogen (c) are approximately the same; at the same time they are significantly longer than that measured for the tF8H2 gradient formed in air (Figures 14b and 15b). Also note that the gradient profiles measured for specimens prepared by diffusing tF8H2 in air across the PDMS ridges (Figures 14b and 15b) are much narrower than the remaining two gradients (Figures 14a and 15a and Figures 14c and 15c). We rationalize the observed behavior as follows. Recall that only minute concentrations of water are needed to hydrolyze the Si−Cl bond, thus converting it into Si−OH.[1] Hydrogen bonds between the hydroxyls from several molecules can be responsible for the formation of relatively stable clusters. Moreover, the long-living nature of such clusters is further facilitated by rather strong intermolecular van der Waals forces acting between two or more $-(CF_2)_8-$ helices.[53,54] Hence, in tF8H2 deposited in air, the molecules likely form clusters comprising several hydrolyzed tF8H2 species. Being heavier than individual tF8H2 molecules, these clusters cannot travel large distances in the vapor phase and therefore deposit at closer proximities to the diffusing source. After "landing" on the substrates, these clusters may further travel along the surface until they get incorporated into the existing SAM via physisorption and finally chemisorption to the substrate (and possibly also participate in the formation of in-plane networks, known to occur in trifunctionalized organosilanes[1,3,4]). The situation is schematically depicted in Figure 16. The formation of mF8H2 in air and tF8H2 in nitrogen is different from that of tF8H2 in air. Neither molecule can form stable clusters; mF8H2 lacks the functionality near the silicon atom, tF8H2 does not get hydrolyzed, and hence, no H-bonds are present that would provide temporary stabilization among the molecules. Therefore, in these situations these SFOs travel throughout the vapor phase primarily as individual molecules; being lighter than the aforementioned complexes formed by hydrolyzing tF8H2 in air, they journey larger distances from the diffusing source and generate broader concentration profiles. Finally, upon impinging on the substrates, the chlorine atoms get converted into hydroxyls. Both types of molecules have a chance to diffuse along the surface, the trifunctional species may form temporary complexes, and finally, they get incorporated into the SAM as described earlier. Again, a schematic representation of the process is depicted pictorially in Figure 16.

(53) Chidsey, C. E. D.; Loiacono, D. N. *Langmuir* **1990**, *6*, 682.
(54) Tamada K.; et al. *Langmuir* **2001**, *17*, 1913−1921.

Conclusions

In this paper we have described the formation and properties of molecular gradients prepared by an evaporation method developed in the early 1990s by Chaudhury and Whitesides.[17] We have demonstrated that the overall deposition process is quite complex, involving several different transport and reaction phenomena. Because of the large battery of parameters governing the formation of such structures, we have limited ourselves to work with SFOs with two different end groups (mono- and trifunctional) and studied how variation of the SFO flux and the structure of the surface affect the characteristics of SFO moieties in the molecular gradients. Surface-sensitive combi-NEXAFS spectroscopy was used to determine the position-dependent concentration and molecular orientation of SFOs in the molecular gradient on surfaces. Using this information, we established correlations between the fraction of the F8H2 species (the grafting density) on the substrate and the average tilt angle of the $-(CF_2)_8F$ group. We further used structured substrates to shed more light on the mechanism of SAM formation in SFOs. Specifically, we have shown that SFO SAMs form primarily by incorporating new SFO species into preexisting semifluorinated molecular templates chemisorbed on surfaces. We have also demonstrated that the mechanism involving the incorporation of SFOs into SAMs depends crucially on the chemical nature of the end group around the silicon atom and the type of vapor. While mF8H2 species add themselves primarily as individual molecules, the incorporation of tF8H2 into surface-bound SAMs depends on the nature of the vapor phase. In an inert gas phase, the addition of tF8H2 follows the same pathway as that of mF8H2 in air (and presumably also in nitrogen gas); in a humid atmosphere tF8H2 hydrolyzes rapidly and forms multimolecular building blocks, which are added to the preexisting SAM.

Acknowledgment. We thank the National Science Foundation for supporting this research. NEXAFS spectroscopy experiments were carried out at the National Synchrotron Light Source, Brookhaven National Laboratory, which is supported by the U.S. Department of Energy, Division of Materials Sciences and Division of Chemical Sciences.

LA061016R